ICARUS 95, 319–324 (1992)

NOTE

Photometric Variability of Charon at 2.2 μm

A. S. BOSH,[1] L. A. YOUNG, J. L. ELLIOT,[1,2] AND H. B. HAMMEL[1]

Department of Earth, Atmospheric, and Planetary Sciences, Massachusetts Institute of Technology, Cambridge, Massachusetts 02139-4307

AND

R. L. BARON

Infrared Telescope Facility, Institute for Astronomy, 2680 Woodlawn Drive, Honolulu, Hawaii 96822-1897

Received August 29, 1991; revised November 27, 1991

Several dozen Pluto–Charon images were obtained on each of 4 nights with the ProtoCAM on the IRTF, mostly at K (2.2 μm) but also at J (1.2 μm) and H (1.7 μm). The seeing at FWHM ranged from 0.45 to 1.06 arcsec. A two-source image model was fit to the blended images of Pluto and Charon, with the position of Charon and the ratio of its signal to that of Pluto as free parameters. At K, we find Charon to be fainter than Pluto by 1.80 ± 0.09, 2.39 ± 0.05, and 2.09 ± 0.05 mag at lightcurve phases 0.06, 0.42, and 0.95. Combining these magnitudes with combined photometry of the Pluto–Charon system we find apparent K magnitudes for Charon of 15.01 ± 0.08 at lightcurve phase 0.06 and 15.46 ± 0.05 at lightcurve phase 0.42. We conclude that Charon is variable in this filter bandpass. The variation is most likely due to changes in its geometric albedo as a function of longitude.

1. Introduction. Understanding the Pluto–Charon "double planet" presents a challenge to current models for Solar System formation (McKinnon 1989, Simonelli and Reynolds 1989). A prerequisite for making progress in this area is knowledge of the individual properties of these bodies: their masses, radii, and compositions. One approach for resolved observations has been the mutual events (Binzel *et al.* 1985). From these Tholen *et al.* (1987) derived values for the radii of Pluto and Charon and their separate albedos. Marcialis *et al.* (1987) and Buie *et al.* (1987) detected the 2.0-μm water ice band on Charon's surface, and Fink and diSanti (1988) established an upper limit on a CH_4 atmosphere on Charon. Speckle interferometry was employed by Beletic *et al.* (1989) to measure the semimajor axis of the Pluto–Charon orbit. Stellar occultations are yet another method for separate observations of these bodies. This technique provided the first direct detection of Pluto's atmosphere and measurement of its scale height (Elliot *et al.* 1989b, Hubbard *et al.* 1988), evidence for a possible atmosphere of Charon (Elliot and Young 1991), and a precise radius for Pluto at the level of unit optical depth (Millis *et al.*, in preparation).

Recently, it has become possible to obtain separate photometry of Pluto and Charon through approaches not limited to two precise orbital phases as are the mutual events. Previous resolved photometry of Pluto and Charon (Albrecht *et al.* 1991, Jones *et al.* 1988, Reitsema *et al.* 1983) has established the magnitude differences of Pluto and Charon at several visible wavelengths, but no attempt has been made to establish separate lightcurves of these bodies. In this note we present infrared imaging observations taken with ProtoCAM on NASA's Infrared Telescope Facility (IRTF) at several orbital phases, which we analyze with model fitting and aperture photometry. From these results we investigate the possibility that Charon has a variegated surface, as has been inferred for Pluto from the mutual events (Binzel 1989) and from the Pluto–Charon lightcurve (Buie and Tholen 1989, Marcialis 1988).

2. Observations. We observed four stellar appulses in May and June 1991 (Dunham *et al.* 1991) with the 62 × 58 pixel ProtoCAM (Toomey *et al.* 1990) on the IRTF, at a nominal focal plane scale of 0.35 arcsec per pixel. The original goal of these observations was to record an occultation by Pluto at infrared wavelengths. Our strategy for these potential occultations concentrated on imaging Pluto–Charon and the appulse star through the K filter. We used an integration time of 50 sec, chosen to maximize the signal-to-noise ratio in Pluto while still integrating for a short enough time to be able to detect an occultation. We "nodded" the telescope after each exposure: in this mode this image was moved between two different areas of the detector on alternate frames. This procedure allowed us to continually record data on Pluto while still recording background information. On each night we obtained several hours of data, including frames of a photometric standard star, and frames of Pluto–Charon and the appulse star. Most data were taken at K (2.2 μm), but on 2 of the nights (May 12 and June 22) we also recorded frames at J (1.2 μm) and H (1.7 μm).

Preliminary astrometric analysis of the data indicates that there were no occultation events on the nights of May 12, May 28, and June 17. This analysis has not been completed for the data from June 22. How-

[1] Visiting Astronomer at the Infrared Telescope Facility, which is operated by the University of Hawaii under contract to the National Aeronautics and Space Administration.

[2] Also Department of Physics, Massachusetts Institute of Technology, Cambridge, Massachusetts 02139-4307.

0019-1035/92 $3.00

TABLE I
Observations

Date	Closest approach (UT)	Photometric quality	Image diameter at FWHM (arcsec)	Focal plane scale (arcsec/pixel)	Angle of north on detector[a] (deg)
1991 May 12	6:12	Excellent	0.91–1.06	0.338 ± 0.007	−89.9 ± 1.0
1991 May 28	12:46	Poor: heavy cirrus	0.80–0.88	0.345 ± 0.006	−95.2 ± 1.5
1991 June 17	10:00	Moderate: light cirrus	0.45–0.68	0.351 ± 0.016	−92.8 ± 0.7
1991 June 22	10:08[b]	Moderate: light cirrus	0.48–0.54	[Not calculated]	

[a] See text for definition of angle convention.
[b] For June 22, the closest approach time listed is the predicted value.

ever, because these data represent snapshots of the Pluto–Charon system at four distinct lightcurve phases, they can be used to provide relative magnitudes of Pluto and Charon for each lightcurve phase observed. Table I summarizes the observing circumstances, while Table II includes the lightcurve phases. The lightcurve phase ranges from 0 to 1, and is defined with respect to the Pluto–Charon system lightcurve (Binzel *et al.* 1985). Column 3 gives an indication of the photometric quality of the night, as recorded by the observer. The next column lists the full width at half-maximum signal (FWHM) of the stellar point-spread function, determined through modeling of Pluto and Charon as a double source. Note that the apparent separation of Pluto and Charon on May 12 and May 28 was 1.0 arcsec; the separation on June 17 was 0.8 arcsec. On June 22 the separation of Pluto and Charon ranged from 0.5–0.6 arcsec which proved too small for easy application of the methods used for the rest of the data set.

In this analysis, we calibrate the focal plane scale and detector orientation relative to the celestial sphere by comparing Pluto's ephemeris to the measured motion of the Pluto–Charon image past the appulse star. We also find the closest approach date and time in this manner. These quantities are given in Table I, where the angle of north is defined to be from the row axis through the column axis (Elliot *et al.* 1989a). For example, if north were parallel to the columns and in the direction of decreasing row number, then the angle of north would be −90°.

3. Relative photometry. In order to learn the ratio of Charon's intensity to that of Pluto and its position relative to Pluto, we developed a two-source model to fit to the images on our ProtoCAM frames. The model incorporates a radially symmetric, Lorentzian point-spread function defined by a peak signal (s_0), an image diameter (d), and a power (p) that specifies the shape of the profile. If r is the distance from the center of the image, then $s(r)$, the signal at r, is given by the equation

$$s(r) = \frac{s_0}{1 + (2r/d)^p}. \quad (1)$$

Note that the image diameter is the FWHM of the image profile. To find the model signal for a given pixel, we integrate Eq. (1) over the pixel area with Gaussian quadrature on a 2 × 2 grid. The maximum difference of this procedure from a more accurate numerical integration is only 0.6% for typical parameters encountered in our data set. The radial extent of our model image had no definite bound, but was limited only by the subset of pixels chosen for analysis.

We modeled the background on the ProtoCAM frames by averaging the background for the image area in the frames taken before and after the frame of interest. The background in each pixel of the average was then multiplied by a model parameter f (near 1.0 and the same for all pixels), which yielded the background value for the frame of interest.

Our complete model of the Pluto–Charon image for a single frame has nine parameters: (1) the background factor f, (2 and 3) the diameter d and power p of the point-spread function, (4, 5, and 6) the peak signal of Pluto's image, and its row and column center, and (7, 8, and 9) the ratio of Charon's signal to that of Pluto, and its row and column center relative to that for Pluto. When this model is used to describe the Pluto–Charon images on a series of frames, each frame had its own value for the first six parameters just described, but a single value was

TABLE II
Model Results for Pluto–Charon Images

Date (1991)	Effective Midtime (UTC)	Frame numbers	Light curve phase	Filter	rms residual per pixel (ADU)	From ephemeris row offset (pixel)	From ephemeris col. offset (pixel)	Fitted parameters* for Charon, relative to Pluto row offset (pixel)	Fitted parameters* for Charon, relative to Pluto col. offset (pixel)	Fitted parameters* for Charon, relative to Pluto Intensity ratio (Sc/Sp)	Magnitude difference (Mc − Mp)
May 12	9:55	217-224	0.433	J	201.9	2.62±0.16	−0.54±0.06	3.15±0.11	−0.22±0.08	0.094±0.009	2.57±0.10
May 12	10:04	225-230	0.433	H	158.4	2.62±0.16	−0.54±0.06	3.06±0.13	−0.29±0.11	0.095±0.008	2.56±0.09
May 12	10:12	231-236	0.434	K	67.6	2.62±0.16	−0.54±0.06	2.98±0.13	−0.16±0.11	0.110±0.010	2.40±0.10
May 12	7:09	69-78	0.415	K	47.0	2.50±0.15	−0.56±0.06	2.67±0.11	−0.92±0.13	0.121±0.008	
May 12	7:20	78-87	0.416	K	44.6	2.51±0.15	−0.56±0.06	2.82±0.13	−0.48±0.10	0.105±0.009	
May 12	8:17	130-139	0.422	K	64.8	2.55±0.15	−0.56±0.06	2.92±0.13	−0.40±0.11	0.106±0.009	
	7:43	average	0.418			2.52±0.15	−0.56±0.06	2.80±0.09	−0.60±0.20	0.111±0.005	2.39±0.05
						(Gaussian results:		2.99±0.08	−0.61±0.22	0.121±0.005)	
May 28	11:34	71-80	0.948	K	41.6	−2.67±0.16	0.26±0.07	−2.83±0.05	0.20±0.05	0.158±0.006	
May 28	11:45	81-90	0.950	K	37.6	−2.67±0.16	0.26±0.07	−2.82±0.06	0.11±0.05	0.146±0.007	
May 28	11:57	91-100	0.951	K	48.3	−2.67±0.16	0.26±0.07	−2.96±0.08	0.06±0.07	0.135±0.008	
	11:46	average	0.950			−2.67±0.16	0.26±0.07	−2.87±0.06	0.12±0.05	0.146±0.007	2.09±0.05
						(Gaussian results:		−2.91±0.03	0.09±0.06	0.162±0.005)	
June 17	7:51	86-95	0.055	K	47.1	−2.38±0.17	0.14±0.03	−2.39±0.03	0.07±0.03	0.201±0.005	
June 17	8:27	110-119	0.059	K	44.1	−2.35±0.17	0.13±0.03	−2.27±0.04	0.05±0.04	0.211±0.008	
June 17	8:59	128-137	0.063	K	59.1	−2.32±0.17	0.12±0.03	−2.38±0.04	−0.21±0.05	0.161±0.008	
	8:25	average	0.059			−2.35±0.17	0.13±0.03	−2.35±0.05	−0.03±0.11	0.191±0.015	1.80±0.09
						(Gaussian results:		−2.43±0.02	0.03±0.03	0.212±0.007)	

[a] Using Lorentzian profile; Gaussian results are included to demonstrate insensitivity to form of point-spread function.

used for the signal ratio of Charon to Pluto and the row and column offset of Charon's image relative to Pluto's.

For each night, we chose three series of 10 consecutive frames each for model fitting, under the assumption that any change in Pluto or Charon is negligible over the 10 min covered by these frames. In addition, we used only frames on which the images of Pluto–Charon and the appulse star were separated by at least 10 pixels. The frame numbers and effective midtimes (UTC) for these frames are listed in the second and third columns of Table II. For each frame we did a least-squares fit of our model to the Pluto–Charon image over an 11 × 11 pixel area, centered on the image. The data for known "bad pixels"—usually two or fewer—on the ProtoCAM array were omitted from the fit (rather than replaced by the average of nearby pixel values). For the three parameters describing the intensity and position of Charon's image, we began with the average of those from the single frame fits. For all other parameters, results of the individual fits were used as starting values for the multiple frame fit (i.e., the parameters describing the backgrounds, point-spread functions, and Pluto images). We find that the residuals of these model fits are approximately normally distributed.

The results of the fits are summarized in columns 6 and 9–12 of Table II. The error bars on the individual entries in columns 9–12 are the formal errors from the fits, but the error bars on the averages were calculated from the scatter of the three quantities used in the average. Columns 7 and 8 list the predicted positions for Charon calculated from its ephemeris (Tholen and Buie 1990), using the value of the semimajor axis given by Beletic *et al.* (1989). The errors in these predicted positions were calculated from the error in the focal plane scale and the error in the semimajor axis inflated above Beletic *et al.*'s (1989) error by the amount recommended by Elliot and Young (1992). The magnitude differences and errors in column 13 were calculated from the intensity ratios in the previous column. The values of p, the power in the Lorentzian model, are not tabulated because they are different for each frame in the multiple frame fit. However, the mean value was 2.8, and the range was 2.15–3.34.

We assess the validity of our results with three approaches: (i) comparison of the fitted Charon positions with those calculated from its ephemeris (Tholen and Buie 1990), (ii) comparison of the scatter of the multiple-fit results with their formal errors, and (iii) comparison of the intensity ratios determined using this Lorentzian image profile with those determined using a Gaussian image profile. As can be seen in Table II, the mean row and column positions for the night of June 17 agree with the ephemeris position within the formal errors. For May 28, the agreement is slightly outside of one standard deviation for the row and column positions. For May 12, the column position agrees, but the row position is slightly outside this bound. The positions from the frames used for the relative JHK photometry agree with the series of three fits used for the K photometry alone. Therefore, in comparing the predicted and fitted Charon offsets, we find that they agree to within a factor of 2 of the formal rms error in the difference. We find a similar situation when comparing the formal error in each intensity ratio with the error calculated from the scatter of three ratios for each night. As these data were taken within 80 min, we assume the ratios should be the same for these sets. Hence we conclude that the real errors for Charon's fitted parameters are within a factor of 2 of the formal errors from the least-squares fits; our adopted magnitude errors are given in Table II.

The third test of the intensity ratios is done by comparing the results described above with those one would get using a Gaussian image profile to determine the intensity ratios. These results are included in Table II for comparison. The fits were performed in the same way as for the Lorentzian image profile fits, except the image profile was modeled by a Gaussian. It is evident from the results in Table II that the intensity ratios obtained with the two methods agree to within a factor of 2 of the errors calculated from the scatter of the data, although the ratios using the Gaussian are consistently about 10% greater than those using the Lorentzian model. For the remainder of this analysis, we will use the results from the Lorentzian model, because these had lower residuals.

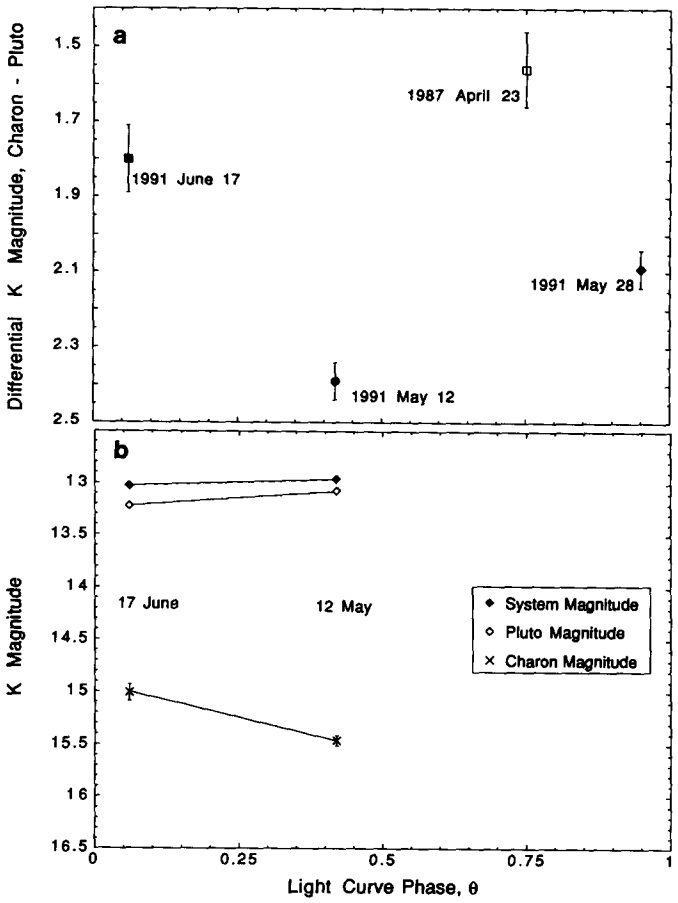

FIG. 1. Pluto and Charon lightcurves. (a) This figure shows the K-magnitude difference between Pluto and Charon as a function of lightcurve phase. Included are results from three of our runs, and one point from Buie *et al.* (1987). (b) This figure shows the separate magnitudes of Pluto and Charon as a function of lightcurve phase. They were determined through a combination of model fitting and aperture photometry, as described in the text. The uncertainties in the system and Pluto magnitudes are approximately the size of the symbol used. Data from May 28 are not plotted in this figure because this night was nonphotometric and we could not calculate system magnitudes. This does not affect the ratios shown in (a). Note that while the system magnitude does not appear to change, Charon's magnitude decreases when it is near southern elongation.

We plot the relative magnitudes of our fits as a function of lightcurve phase in Fig. 1a. The error bars plotted are from the scatter of the ratios. We also include in this figure a point derived from Buie *et al.* (1987) by integrating their published separate magnitudes of Pluto and Charon over the bandpass of the K filter. Note that our relative magnitudes differ by much more than their errors, implying a short-term variability. Also, the magnitude difference from Buie *et al.* (1987) is much lower than any of ours, perhaps implying a longer-term variability or a lightcurve with an amplitude of 1 mag.

4. System photometry. The model fitting described above provides the brightness ratio of Pluto and Charon, but in order to apportion the variation to each member of the system, we first need the results from

combined photometry of Pluto and Charon. For each night, we reduced all frames for which Pluto–Charon and the appulse star were separated by more than 10 pixels (typically greater than 1 h from closest approach). Since the data from the night of June 22 were not included in the model fits, these data were not included in this photometric analysis. The number of Pluto–Charon frames reduced on the other 3 nights are 72, 40, and 42. Additionally, data were reduced for the standard star BD + 2°2957 (Elias *et al.* 1982) and for the secondary standard star 945FK4.

The photometry was performed by first subtracting pairs of frames, since each member of the pair provided the background measurement for the other. These subtracted frames were then corrected for bad pixels by replacing each such pixel with the average of its four nearest neighbors. (We knew the location of bad pixels before taking the data, so only occasionally did an image fall on one.) An image area was defined to be 10 × 10 pixels, centered on the image. Because the pairs of frames could differ in mean level by a few percent, an additional background subtraction was performed. A background area was defined to be the square "annulus" formed by subtracting the previously defined image area from a 14 × 14 pixel area. In most cases, the background area was centered on the image also, but occasionally bad pixels or other nearby images forced the background area to be offset from the image center. Bad pixels were not included in the background value determination. Additionally, background pixel values that deviated by more than 3σ from the mean background value were removed from the background area, in order to avoid spurious data values (e.g., cosmic ray hits).

The star signal was determined by summing the pixel values in the image area and then subtracting the mean background value, scaled to the number of pixels in the image area. The noise was assumed to be background limited, and was calculated from the standard deviation of the background pixel values. The magnitudes for Pluto–Charon and the appulse stars were then derived in the standard way. Possible sources of error in the signal determination are uncorrected nonlinearity and the lack of flattening. The nonlinearity (Ressler, personal communication) would affect only the signal from the standard stars, since the signal levels from Pluto–Charon and the appulse stars were too low. A test showed that linearizing the standard stars would change the signal levels by only 0.5% or 0.006 mag, a magnitude difference that is much smaller than our errors. We did not flatten because the images of Pluto–Charon and the standard stars were always on the same areas of the detector.

While determining the extinction, we found that the night of May 28 was not photometric. Therefore, we did not calculate system magnitudes for this night. The fact that this night was not photometric should not affect the Pluto–Charon signal ratios determined from the model fitting because the images of Pluto and Charon were within an arcsecond of each other. For the night of May 12, we find a K extinction coefficient of 0.211 ± 0.075 for the odd-numbered frames, and 0.181 ± 0.044 for the even-numbered frames. For the night of June 17, we find 1.189 ± 0.389 for the odd-numbered frames, and 0.643 ± 1.019 for the even-numbered frames. These coefficients are given separately for the odd- and even-number frames because the image appeared on one of two positions on the chip due to the "nodding" of the telescope during data acquisition. These two chip positions appear to have different responses; therefore, one area of the chip has an intrinsically lower signal-to-noise ratio than the other. Note that the magnitude of the extinction coefficients for the two areas agrees to within the errors. We calculate the extinction coefficients separately in order to preserve the signal-to-noise ratio of the better area of the chip. Also note that the extinction coefficient for the night of June 17 is much larger than usual, with correspondingly large errors. Since this is time-series photometry, rather than all-sky photometry, this large coefficient may indicate a sensitivity drift, or some other time-variable response. However, on this night (as well as May 12), the standard star used was less than 4° from Pluto, and was observed close in time to the Pluto observations. Over this small angular and temporal distance, any variations in extinction or response will be small, and additionally will be well represented by the errors in the derived coefficient.

The reduction of these data gives apparent K magnitudes for the combined light of Pluto and Charon of 12.95 ± 0.01 for May 12.3215, and 13.03 ± 0.03 for June 17.3507. Note that these magnitudes are not corrected to a standard solar phase angle, since this correction is uncertain for these wavelengths, and the solar phase angles spanned by these observations are sufficiently constrained that any relative differences will be small. Using these combined magnitudes and the Charon–Pluto ratios determined from model fitting, we find the individual magnitudes for Pluto and Charon. In Fig. 1b, the separate magnitudes of Pluto and Charon, and the system magnitude are plotted against lightcurve phase. Note that while the Pluto–Charon system magnitude is consistent with a flat lightcurve to within our errors, Charon is fainter at lightcurve phase 0.42 (near southern elongation).

In order to determine geometric albedos from these magnitudes, we adopted radii from Elliot and Young (1992) of 1206 ± 11 km for Pluto and the lower limit of 602 ± 1 km for Charon (Elliot and Young 1991). Using the solar magnitude at K from Campins *et al.* (1985), we find the individual geometric albedos at K of Pluto and Charon at lightcurve phase 0.42 to be 0.33 ± 0.01 and 0.15 ± 0.01, respectively; at lightcurve phase 0.06, we find 0.29 ± 0.01 and 0.23 ± 0.02.

5. Discussion. We now consider our results in the context of previous resolved photometry, which has been performed at several wavelengths, but each at a single lightcurve phase (see Fig. 2). Reitsema *et al.* (1983) used image deconvolution to determine the magnitude difference between Pluto and Charon in their 1980 observations. In 1987, Marcialis *et al.* (1987) determined the individual fluxes of Pluto and Charon at four wavelengths during a mutual event. Buie *et al.* (1987) obtained individual spectra using a circular variable interference filter (CVF) during a mutual event in 1987. In April 1987, Binzel (1988) observed a Pluto–Charon mutual event in B and V, yielding separate magnitudes at these two wavelengths. Jones *et al.* (1988) observed the Pluto system in 1987, and used DAOPHOT (Stetson 1987) to obtain separate magnitudes for Pluto and Charon. In 1990, Albrecht *et al.* (1991) observed Pluto and Charon with the Faint Object Camera aboard the Hubble Space Telescope. Using image deconvolution, they determined the individual magnitudes of Pluto and Charon at wavelengths of 3420 and 4300 Å.

Figure 2 displays Pluto–Charon differential magnitudes as a function of wavelength. We emphasize that there are several lightcurve phases involved. This figure includes three data sets in the infrared: this work, Marcialis *et al.* (1987), and Buie *et al.* (1987). The measurements of Marcialis *et al.* (1987) and Buie *et al.* (1987) are high-resolution; thus, they do not directly compare with our measurements that lie in the same wavelength region. The bandpasses for the broadband and high-resolution filters are plotted at the bottom of this figure. Note the differences among the Jones *et al.* (1988) and Albrecht *et al.* (1991) points in the visible and near UV, even though they are within a lightcurve phase range of 0.01. The data from Reitsema *et al.* (1983) and Binzel (1988) lie in the same wavelength region, but are at different lightcurve phases.

It is difficult to interpret the differences among these relative magnitudes due to the number of variables involved: wavelength, bandpass, lightcurve phase, solar phase angle, and Pluto–Charon season. Further, the way in which the relative magnitudes change with respect to these variables depends on the individual magnitude variations of both Pluto and Charon. These variations may have contributions from four sources: rotation, orientation of the pole, solar phase angle, and season. Magnitude differences associated with rotation and orientation can be caused by changes in surface albedo with latitude and longitude, and the less likely possibility that Pluto or Charon is oblate. Unless Charon is in asynchronous rotation, these will have the same period as the Pluto–Charon system lightcurve. The relative magnitude will depend on solar phase angle if Pluto and Charon have different solar phase relations. Because Pluto and Charon are in an eccentric solar orbit, there may be seasonal changes in albedo on either body that occur over time scales of decades due to sublimation, condensation, or redistribution of surface ices.

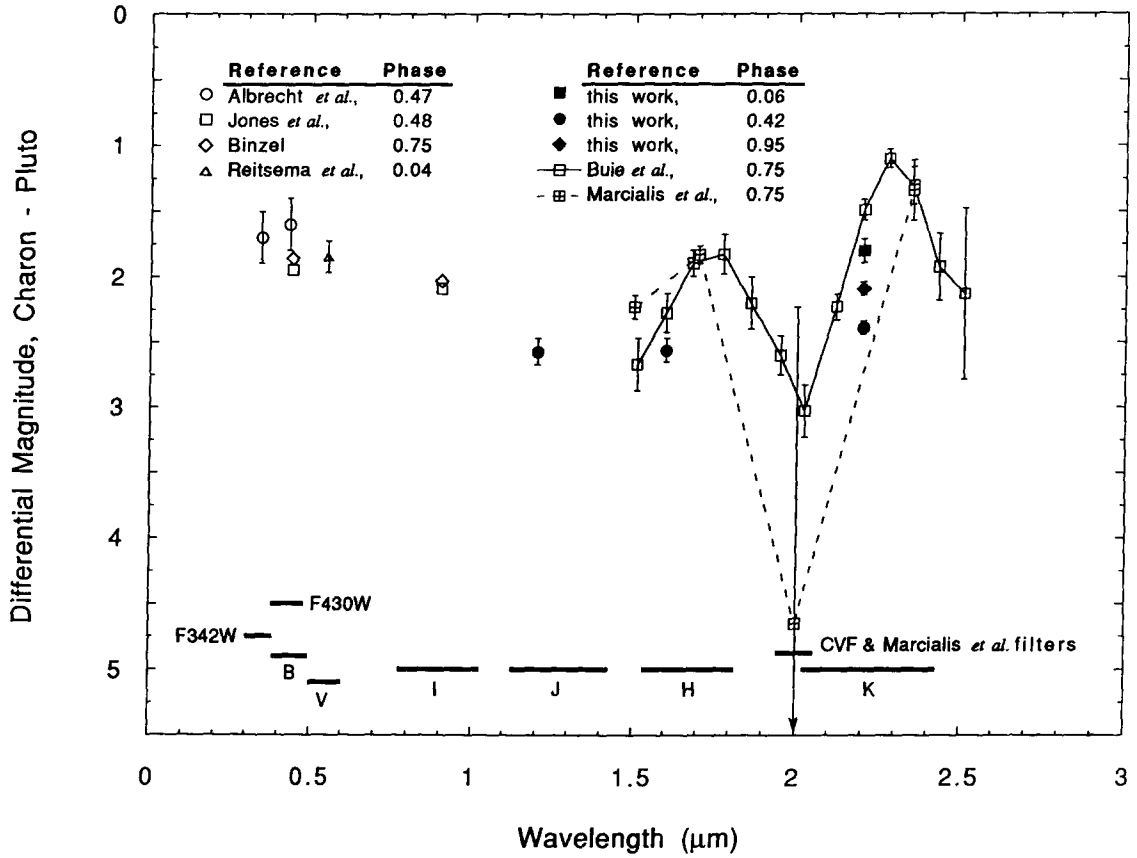

FIG. 2. Spectrum of the Pluto–Charon magnitude difference. As described in the text, the available data are plotted in this figure as a function of wavelength. Note that the uncertainty in the values of Jones *et al.* (1988) and Binzel (1988) are approximately the size of the symbol used. Lightcurve phase is indicated in the legend. Bandpasses for the filters are indicated at the bottom of the plot. The points are plotted at the mean wavelength of the filter, which for J and H does not coincide with the midpoint of the filter. The filters used by Albrecht *et al.* (1991) are labeled "F342W" and "F430W."

Of the variables mentioned above, the only ones that affect the individual Charon magnitudes over the short time interval spanned by our observations are wavelength, lightcurve phase, and solar phase angle. Assuming that the magnitude of the infrared phase correction is similar to that in the visible, 0.04 mag deg^{-1} (Binzel and Mulholland 1983), solar phase effects would not exceed 0.04 mag for our data. Hence the most likely source of our detected variation of Charon is due to albedo differences on its surface.

Water ice has been detected on Charon at light-curve phase 0.75 by Marcialis *et al.* (1987) and Buie *et al.* (1987), who found no evidence for methane. This, combined with our analysis, suggests that Charon has different amounts of water ice on its surface, but does not rule out the possibility of variation due to methane ice or other materials. The K filter (2.03 to 2.42 μm) is too broad to distinguish between variation due to the 2.3-μm methane band or to the 2.0-μm water band, as it includes a significant fraction of both bands as well as part of the weaker 2.4-μm water band. Although methane was not detected on one hemisphere of Charon, it may exist on the other hemisphere or may be transient. It has been argued that methane cannot exist on Charon (Trafton *et al.* 1988); however, the individual masses of Pluto and Charon are sufficiently uncertain that Charon's surface gravity could nearly equal Pluto's (Elliot and Young 1991). If this were the case, methane ice could exist on Charon and contribute to its photometric variability.

A major implication of Charon's variability is that one simplifying assumption—that all of the system variability comes from Pluto—should be reexamined for each wavelength. In particular, the lightcurve of Charon needs to be determined for visible wavelengths, because the "spot" albedo models (Buie and Tholen 1989, Marcialis 1988) depend on this assumption.

6. Conclusions. We have determined individual magnitudes of nearly opposite hemispheres for both Pluto and Charon in the K filter. Charon varies by 0.45 ± 0.09 mag between these two hemispheres. This change is most likely due to a difference in the strength of the 2.0-μm water absorption band on the two hemispheres.

More rotational and spectral coverage is needed to decouple the contributions of Pluto and Charon to the system lightcurve and to determine their individual variabilities more fully. This is particularly important at visible wavelengths, where the system lightcurve has been attributed entirely to Pluto and used to construct "spot" models for Pluto. These observations can be improved by using a brighter appulse star. In addition, observations should be made with filters that measure flux from the water or methane bands alone in order to determine the cause of the magnitude difference observed in this work. Characterizing and understanding the causes of the photometric variations will lead to an improved understanding of the individual properties of Pluto and Charon.

ACKNOWLEDGMENTS

We thank M. Sykes and M. Buie for their comments as referees, D. Tholen for use of his "ephem" program, and M. Ressler for supplying

the linearization code. We are also grateful to the IRTF staff, with particular thanks to the telescope operators B. Golisch, D. Griep, and C. Kaminski. This work was supported, in part, by NASA Grant NAGW-1494 and NSF Grant AST-8906011. Also, ASB is partially supported by the NASA Graduate Student Researchers Program.

REFERENCES

ALBRECHT, R., C. BARBIERI, J. C. BLADES, A. BOKSENBERG, P. CRANE, J. M. DEHARVENG, M. J. DISNEY, P. JAKOBSEN, T. M. KAMPERMAN, I. R. KING, F. MACHETTO, C. D. MACKAY, F. PARESCE, G. WEIGELT, D. BAXTER, P. GREENFIELD, R. JEDRZEJEWSKI, A. NOTA, AND W. B. SPARKS 1991. First results from the faint object camera: High-resolution imaging of the Pluto–Charon system. *Astrophys. J.* **374,** L65–L67.

BELETIC, J. W., R. M. GOODY, AND D. J. THOLEN 1989. Orbital elements of Charon from speckle interferometry. *Icarus* **79,** 38–46.

BINZEL, R. P. 1988. Hemispherical color differences on Pluto and Charon. *Science* **241,** 1070–1072.

BINZEL, R. P. 1989. Pluto–Charon mutual events. *Geophys. Res. Letters* **16,** 1205–1208.

BINZEL, R. P., AND J. D. MULHOLLAND 1983. Photometry of Pluto during the 1982 opposition. *Icarus* **88,** 222–225.

BINZEL, R. P., D. J. THOLEN, E. F. TEDESCO, B. J. BURATTI, AND R. M. NELSON 1985. The detection of eclipses in the Pluto–Charon system. *Science* **228,** 1193–1195.

BUIE, M. W., D. P. CRUIKSHANK, L. A. LEBOFSKY, AND E. F. TEDESCO 1987. Water frost on Charon. *Nature* **329,** 522–523.

BUIE, M. W., AND D. J. THOLEN 1989. The surface albedo distribution of Pluto. *Icarus* **79,** 23–37.

CAMPINS, H., G. H. RIEKE, AND M. J. LEBOFSKY 1985. Absolute calibration of photometry at 1 through 5 μm. *Astron. J.* **90,** 896–899.

DUNHAM, E. W., S. W. MCDONALD, AND J. L. ELLIOT 1991. Pluto–Charon stellar occultation candidates: 1990–1995. *Astron. J.* **102,** 1464–1484.

ELIAS, J. H., J. A. FROGEL, K. MATTHEWS, AND G. NEUGEBAUER 1982. Infrared standard stars. *Astron. J.* **87,** 1029–1034.

ELLIOT, J. L., E. W. DUNHAM, R. L. BARON, A. W. WATTS, S. P. KRUSE, W. R. ROSE, AND C. M. GILLESPIE 1989a. Image quality of the Kuiper Airborne Observatory. I. Results of the first flight series. *Publ. Astron. Soc. Pacific* **101,** 737–764.

ELLIOT, J. L., E. W. DUNHAM, A. S. BOSH, S. M. SLIVAN, L. A. YOUNG, L. H. WASSERMAN, AND R. L. MILLIS 1989b. Pluto's atmosphere. *Icarus* **77,** 148–170.

ELLIOT, J. L., AND L. A. YOUNG 1991. Limits on the radius and a possible atmosphere of Charon from its 1980 stellar occultation. *Icarus* **89,** 244–254.

ELLIOT, J. L., AND L. A. YOUNG 1992. Analysis of stellar occultation data for planetary atmospheres. I. Model fitting, with application to Pluto. *Astron. J.* **103** in press.

FINK, U., AND M. A. DISANTI 1988. The separate spectra of Pluto and its satellite Charon. *Astron. J.* **95,** 229–236.

HUBBARD, W. B., D. M. HUNTEN, S. W. DIETERS, K. M. HILL, AND R. D. WATSON 1988. Occultation evidence for an atmosphere on Pluto. *Nature* **336,** 452–454.

JONES, J. H., C. A. CHRISTIAN, AND P. WADDELL 1988. Resolved CCD photometry of Pluto and Charon. *Publ. Astron. Soc. Pacific* **100,** 489–495.

MARCIALIS, R. L. 1988. A two-spot albedo model for the surface of Pluto. *Astron. J.* **95,** 941–947.

MARCIALIS, R. L., G. H. RIEKE, AND L. A. LEBOFSKY 1987. The surface composition of Charon: Tentative identification of water ice. *Science* **237,** 1349–1351.

MCKINNON, W. B. 1989. On the origin of the Pluto–Charon binary. *Astrophys. J.* **344,** L41–L44.

MILLIS *et al.*, in preparation.

REITSEMA, H. J., F. VILAS, AND B. A. SMITH 1983. A charge-coupled device observation of Charon. *Icarus* **56,** 75–79.

SIMONELLI, D. P., AND R. T. REYNOLDS 1989. The interiors of Pluto and Charon: Structure, composition, and implications. *Geophys. Res. Letters* **16,** 1209–1212.

STETSON, P. B. 1987. DAOPHOT: A computer program for crowded-field stellar photometry. *Publ. Astron. Soc. Pac.* **99,** 191–222.

THOLEN, D. J., AND M. W. BUIE 1990. Further analysis of the Pluto–Charon mutual event observations—1990. *Bull. Am. Astron. Soc.* **22,** 1129.

THOLEN, D. J., M. W. BUIE, R. P. BINZEL, AND M. L. FRUEH 1987. Improved orbital and physical parameters for the Pluto–Charon system. *Science* **237,** 511–514.

TOOMEY, D. W., M. SHURE, E. M. IRWIN, AND M. E. RESSLER 1990. ProtoCAM—An innovative IR camera for astronomy. *Proc. SPIE* **1235.**

TRAFTON, L., S. A. STERN, AND G. R. GLADSTONE 1988. The Pluto–Charon system: The escape of Charon's primordial atmosphere. *Icarus* **74,** 108–120.